Composite Structures, 98:242–252, 2013.

Benchmark Solution for Degradation of Elastic Properties due to Transverse Matrix Cracking in Laminated Composites

E. J. Barbero[1] and F. A. Cosso [2]
Mechanical and Aerospace Engineering, West Virginia University, Morgantown, WV 26506-6106, USA

abstract

Degradation of laminate moduli and laminate coefficients of thermal expansion, as well as degradation of the cracked lamina moduli and lamina coefficients of thermal expansion, are predicted as a function of crack density for laminated composites with intralaminar matrix cracks. The methodology assumes linear elastic behavior and periodicity of the transverse cracks. The representative volume element is discretized into finite elements. Stress free conditions on the crack surfaces are enforced. Periodic boundary conditions are applied so that any state of applied far-field strain can be simulated. An averaging procedure is used to yield the average stress field. Three uniaxial states of strain and a null state of strain coupled with a unit increment of temperature are used to obtain the degraded stiffness and coefficients of thermal expansion. Results are presented for a number of laminates and materials systems that are customarily used in the literature for experimentation. The modeling approach and results can be used to assess the quality of approximate models. Comparisons are presented to the predictions of one such model and to experimental data. Also, comparisons are presented to classical lamination theory for asymptotic values of crack density.

keyword

Toughness; Intralaminar; Damage; Periodicity; Thermal Expansion.

1 Introduction

Numerous approximate methods have been developed to predict the onset and evolution of transverse matrix cracking in laminated composites. Micromechanics of Damage Models (MMD) find an approximate elasticity solution for a laminate with a discrete crack or cracks [1–22]. Crack Opening Displacement (COD) models [23–30] are based on the theory of elastic bodies with voids [31]. The methods are approximate because kinematic assumptions are made, such as a linear [32] or bilinear [33] distribution of intralaminar shear stress through the thickness of each lamina, as well as particular spatial distributions of inplane displacement functions [21], stresses, and so on.

[1]Corresponding author. The final publication is available at http://dx.doi.org/10.1016/j.compstruct.2012.11.009

[2]Graduate Research Assistant.

The predictions attained with various approximate methods have been compared in the literature to available experimental data in order to assess the quality of the predictions. Since experimentation is very difficult and laborious, validations are limited to comparing crack density vs. laminate strain (or stress) and laminate modulus reduction vs. laminate strain (or stress). No data exists regarding, for example, degradation of the coefficients of thermal expansion at lamina and laminate levels. Ply degradation has to be inferred from laminate modulus reduction. Since physically observing and counting off-axis cracks is very difficult, the measured crack density is limited to that observed in a single lamina (a 90 deg ply) with the cracks perpendicular to the load direction. However, the available approximate methods are able to predict damage in off axis plies, as well as degradation of shear modulus and Poisson's ratio at the ply level. Unfortunately, those predictions cannot be validated easily.

Several authors have compared approximate solutions to finite element simulations [12, 26, 29, 34–36]. Along those lines, this work proposes a finite element analysis methodology that provides a numerical solution to the 3D equations of elasticity for cracked laminated composites with no additional assumptions other than linear elastic material and periodically spaced cracks. The objective is to produce solutions for a number of responses that are very difficult to tackle experimentally. These solutions could then be used as a benchmark to evaluate the quality of the approximations in various models. As an illustration, the solutions obtained in this work are compared to discrete damage mechanics (DDM) solutions [50]. Also, comparisons to experimental data are presented. Most of the predictions for laminate #1 and #6 are reported herein, and all the results for all six laminates listed in Table 1 are provided as supplementary materials in the online edition of the manuscript.

The model is set up to predict the reduction of stiffness and CTE when only two symmetrically located laminas contain periodically spaced transverse cracks. This is sufficient to validate the approximate models in the literature. Once the reduction of stiffness and CTE for this case is obtained, it is possible to use a CDM approach to address the general case of multiple laminas cracking [50], but such a study is beyond the scope of this work.

2 Periodicity and Homogenization

Since all the approximate methods assume linear elastic material, the proposed methodology retains such assumption, but it must be noted that linearity can be easily removed in the context of finite element analysis (FEA). Next, the proposed methodology assumes that transverse (matrix) cracks occupy the entire ply thickness, are periodically spaced, and are infinitely long along the fiber direction. Once again, these are common assumptions among the approximate models for which we wish to provide a benchmark solution. The justification for these geometric assumptions are well documented in the literature, e.g., [37, Section 7.2.1]. As a result of periodicity, a representative volume element (RVE) is selected and analyzed. The RVE includes the entire thickness of the laminate, it spans the distance between two consecutive cracks, and it has a unit length along the fiber direction (Figure 1). Symmetric laminates subjected to membrane loads are chosen as these are common laminate and load configurations used in virtually all experiments and approximate modes in the literature. A generalization to flexural deformation is possible but not trivial.

Periodicity conditions are carefully applied and verified in such a way that the volume average $\overline{\epsilon}_i$ of the inhomogeneous strain field inside the RVE equals the applied applied strain ϵ_i^0. Other boundary conditions (b.c.) faithfully reflect the stress free condition at the crack surfaces and also allow for the application of any state of far field strain. The analysis yields inhomogeneous strain and stress fields from which it is possible to calculate the degraded stiffness matrix of the laminate.

To calculate the degraded stiffness matrix of the laminate when lamina (k) is cracked, the RVE is subjected to an average strain $\bar{\epsilon}_i$, where $i = 1, 2, 4, 5, 6$, using Voigt contracted notation in the the coordinate system (c.s.) of the cracked lamina. The c.s. of the cracked lamina is chosen so that the stress free b.c. at the crack surface are easily applied. With reference to Figure 1, the averaged strain is applied by enforcing the following b.c. on the displacements

$$\begin{array}{rl} u\left(\frac{1}{2}, y, z\right) - u\left(-\frac{1}{2}, y, z\right) = \epsilon_1^0 & \quad -\frac{1}{2\lambda} \leq y \leq \frac{1}{2\lambda} \\ v\left(\frac{1}{2}, y, z\right) - v\left(-\frac{1}{2}, y, z\right) = \epsilon_6^0 & \quad -\frac{t}{2} \leq z \leq \frac{t}{2} \\ w\left(\frac{1}{2}, y, z\right) - w\left(-\frac{1}{2}, y, z\right) = \epsilon_5^0 & \end{array} \tag{1}$$

and

$$\begin{array}{rl} u\left(x, \frac{1}{2\lambda}, z\right) - u\left(x, -\frac{1}{2\lambda}, z\right) = \frac{1}{\lambda}\epsilon_6^0 & \quad -\frac{1}{2} \leq x \leq \frac{1}{2} \\ v\left(x, \frac{1}{2\lambda}, z\right) - v\left(x, -\frac{1}{2\lambda}, z\right) = \frac{1}{\lambda}\epsilon_2^0 & \quad -\frac{t}{2} \leq z \leq \frac{t}{2} \\ w\left(x, \frac{1}{2\lambda}, z\right) - w\left(x, -\frac{1}{2\lambda}, z\right) = \frac{1}{\lambda}\epsilon_4^0 & \end{array} \tag{2}$$

where t is the thickness of the laminate, $\lambda = 1/(2l)$ is the crack density for cracks spaced a distance $2l$. Note that the applied strains ϵ_i^0 result in average strains $\bar{\epsilon}_i$.

Equation (1) is applied on faces with normal in the x-direction and (2) is applied on faces with normal in the y-direction. Note that the x-direction is the fiber direction of the cracked lamina. Since the laminate is in a state of plane stress, no b.c. are imposed in the z-direction.

In finite element analysis, equations such as (1) are applied via constraint equations (c.e.) between the master node on one face and the slave node on the opposite face. In three dimensional (3D) analysis, every node has three degrees of freedom (dof) representing the displacements u, v, w at the node. By specifying a fixed relationship between two nodes at opposite faces, the slave dof is eliminated. With reference to (1), if the x-face with normal in the positive direction of x, which is called $+x$-face, is chosen as master surface, then the dof u, v, w, are eliminated at the slave, $-x$-face.

Both (1) and (2) apply at the four edges where the $\pm x$-faces and $\pm y$-faces intersect, but the equations cannot be applied independently, as it is done for the faces, because applying (1) eliminates the slave dof that are necessary to apply (2) at the same edges, i.e., at edges where intersecting faces share the same dof. The solution for this problem is to combine (1) and (2) [38, p. 155], in such a way that both boundary equations can be applied simultaneously between a master/slave pair of edges. It turns out that this is only possible among for diagonally opposite edges.

With reference to Figure 2, for edges XpYp (master) and XmYp (slave), equations (1) and (2) are added together, as follows

$$\begin{array}{rl} u\left(\frac{1}{2}, \frac{1}{2\lambda}, z\right) - u\left(-\frac{1}{2}, -\frac{1}{2\lambda}, z\right) = \varepsilon_1^0 + \frac{1}{\lambda}\varepsilon_6^0 & \\ v\left(\frac{1}{2}, \frac{1}{2\lambda}, z\right) - v\left(-\frac{1}{2}, -\frac{1}{2\lambda}, z\right) = \varepsilon_6^0 + \frac{1}{\lambda}\varepsilon_2^0 & \quad -\frac{t}{2} \leq z \leq \frac{t}{2} \\ w\left(\frac{1}{2}, \frac{1}{2\lambda}, z\right) - w\left(-\frac{1}{2}, -\frac{1}{2\lambda}, z\right) = \varepsilon_5^0 + \frac{1}{\lambda}\varepsilon_4^0 & \end{array} \tag{3}$$

For edges XmYp (master) and XpYm (slave), equations (1) and (2) are subtracted from each other, as follows

$$\begin{array}{rl} u\left(\frac{1}{2}, -\frac{1}{2\lambda}, z\right) - u\left(-\frac{1}{2}, \frac{1}{2\lambda}, z\right) = \varepsilon_1^0 - \frac{1}{\lambda}\varepsilon_6^0 & \\ v\left(\frac{1}{2}, -\frac{1}{2\lambda}, z\right) - v\left(-\frac{1}{2}, \frac{1}{2\lambda}, z\right) = \varepsilon_6^0 - \frac{1}{\lambda}\varepsilon_2^0 & \quad -\frac{t}{2} \leq z \leq \frac{t}{2} \\ w\left(\frac{1}{2}, -\frac{1}{2\lambda}, z\right) - w\left(-\frac{1}{2}, \frac{1}{2\lambda}, z\right) = \varepsilon_5^0 - \frac{1}{\lambda}\varepsilon_4^0 & \end{array} \tag{4}$$

Since the $\pm z$-faces are free, the eight vertices can be constrained along with their edges [38, p. 163]. To aid in the programming of the Python script used to automate the modeling, the edges are labeled as the faces that define them (see Fig. 2).

3 Laminate Stiffness and Coefficient of Thermal Expansion

In the context of this manuscript, the objective of homogenization is to obtain the apparent stiffness of a homogenized material where the crack is not geometrically present but having its effect represented by an apparent, degraded stiffness Q. In this work, it is assumed that all cracks are subjected to a combination of tensile and shear loads, without compression. For a discussion of the effects of interfacial crack compression, see [39, 40].

The point wise, linear, elastic constitutive equation, with $\Delta T = 0$, is

$$\sigma = \widetilde{Q} : \epsilon \tag{5}$$

where $\widetilde{Q}$ is the virgin stifness. A volume average is defined as

$$\overline{\phi} = \frac{1}{V} \int_V \phi \; dV \tag{6}$$

The apparent stiffness Q is defined in such a way that it relates the average stress and strain over the volume V of the RVE as follows

$$\overline{\sigma} = Q : \overline{\epsilon} \tag{7}$$

The volume $V = V_S + V_V$ encompasses the volume of the solid V_S plus the volume of the void V_V left by the opening of the crack. If a single crack is placed in the center of the periodic RVE, V_V is the volume of the void from that single crack. If the periodic RVE is defined between two successive cracks, as it is done in this work, then V_V is composed of two half volumes of the cracks on the boundary.

The average strain over the RVE can be decomposed into the strain in the solid plus the deformation of the void

$$\overline{\epsilon} = \frac{1}{V} \int_{V_S} \epsilon \; dV_S + \frac{1}{V} \int_{\partial V_V} u \otimes n \; dV_V \tag{8}$$

where $u, n, \otimes$, are the displacement vector, the outward unit normal to the void surface, and the symmetric dyadic product operator, respectively. The first term on the RHS is not equal to the applied strain ϵ^0, as it is clearly explained in [39, Eq. (2)]. Once the deformation of the void is added, the total average is equal to the applied strain ϵ^0 [41].

Since the stress inside the void is zero, the average stress over the RVE is

$$\overline{\sigma}_i = \frac{1}{V} \int_{V_S} \sigma_i \; dV_S \tag{9}$$

Substituting ϵ^0 for $\overline{\epsilon}$ in (3), the columns of the apparent stiffness Q can be obtained by calculating the average stress for a canonical set of applied strains, namely

$$Q_{ij} = \frac{1}{V} \int_{V_S} \sigma_j \; dV_S \quad ; \quad \epsilon_j^0 = 1 \tag{10}$$

Since transverse matrix cracking primarily affects the inplane properties [26], the intact properties can be used for the intralaminar components of the stiffness, i.e., Q^*_{ij} with $i, j = 4, 5$ [37, (5.47)].

The components of the degraded stiffness matrix Q_{ij} are found by solving the discretized model of the RVE subjected to three loading cases, where only one component of the in-plane strain $\overline{\epsilon}_j$ is different from zero at a time [38, (6.18)] and $\Delta T = 0$. By choosing a unit value of applied strain, and taking into account the enforced state of plane stress, the degraded stiffness matrix is found as

$$Q_{ij} = \frac{\lambda}{t} \int_V \sigma_i dV \quad ; \quad \text{with } \epsilon_j^0 = 1; \quad \Delta T = 0 \tag{11}$$

For each of the three cases, the stress σ_i is computed by the FEA code and the components of the averaged stress $\overline{\sigma}_i$ are calculated by a post processing script that evaluates the volume integrals within each element using Gauss quadrature, then adds them for all the elements, and divides the result by the volume of the RVE.

The first column of Q_{ij} is obtained by applying a strain $\epsilon^0 = \{1, 0, 0, 0, 0\}$ on the boundary (faces and edges), using (1)-(2). The second column of Q_{ij} is obtained by applying a strain $\epsilon^0 = \{0, 1, 0, 0, 0\}$. The third column of Q_{ij} is obtained by applying a strain $\epsilon^0 = \{0, 0, 0, 0, 1\}$. In all three cases, the b.c. are periodic for all laminas and stress free on the cracked surfaces.

Next, periodic boundary conditions simulating zero strain at the uncracked laminas, stress free conditions at the cracked lamina, and a unit change of temperature $\Delta T = 1$ over the entire laminate, allowing us to obtain the average thermal stress field as

$$\overline{\sigma}_i^{thermal} = \frac{\lambda}{t} \int_V \sigma_i dV \quad ; \quad \text{with } \epsilon_j = 0 \quad \forall j; \quad \Delta T = 1; \quad i = 1, 2, 6 \tag{12}$$

Once the averaged thermal stress is known, the laminate coefficient of thermal expansion (CTE) of the laminate is calculated as

$$\alpha_i = Q_{ij}^{-1} \; \overline{\sigma}_j^{\text{thermal}} \tag{13}$$

Once the laminate stiffness Q_{ij} in the c.s. of the laminate is known, the laminate moduli are computed using [37, (6.35)],

$$\begin{aligned} E_x &= \frac{Q_{11}Q_{22} - Q_{12}^2}{Q_{22}} & \qquad G_{xy} &= Q_{66} \\ E_y &= \frac{Q_{11}Q_{22} - Q_{12}^2}{Q_{11}} & \qquad \nu_{xy} &= \frac{Q_{12}}{Q_{22}} \end{aligned} \tag{14}$$

The energy release rate (ERR) is a quantity of interest for predicting the onset of intralaminar cracks and the subsequent evolution of crack density. To calculate the ERR, it is convenient to use the laminate stiffness Q_{ij} in the c.s. of the cracked lamina, because in this way, the ERR can be decomposed into opening and shear modes. Since the laminate stiffness is available from the analysis as a function of crack densityλ, the ERR can be calculated, for a fixed strain level (load), as

$$G_I = \frac{V}{2\Delta A} \left(\epsilon_2 - \alpha_2 \Delta T\right) \Delta Q_{2j} \left(\epsilon_j - \alpha_j \Delta T\right) \quad ; \quad \text{opening mode} \tag{15}$$

$$G_{II} = \frac{V}{2\Delta A} \left(\epsilon_6 - \alpha_6 \Delta T\right) \Delta Q_{6j} \left(\epsilon_j - \alpha_j \Delta T\right) \quad ; \quad \text{shear mode} \tag{16}$$

where $V, \Delta A$, are the volume of the RVE and the increment of crack area, respectively; ΔQ_{ij} is the change in laminate stiffness corresponding to the change in crack area experienced; and all quantities are *laminate average* quantities expressed in the c.s of the cracked lamina in order to allow for ERR mode decomposition [18]. It can be seen that the proposed methodology provides the key ingredients for the computation of the ERR; namely the degraded stiffness and degraded CTE of the laminate, both as a function of crack density.

4 Lamina Stiffness and CTE

Unlike approximate methods, in this work the degraded stiffness of the cracked lamina is calculated directly by averaging the stress field in the cracked lamina. The procedure is identical to that for the laminate but integrating over the volume of the lamina

$$Q_{ij}^{(k)} = \frac{\lambda}{t_k} \int_{V_k} \sigma_i dV \quad ; \quad \text{with } \epsilon_j = 1 \tag{17}$$

where t_k, V_k, are the thickness and volume of the cracked lamina, respectively. Since this is done simultaneously with the analysis of the laminate, there is no additional computational cost or any additional assumption involved.

Once the degraded stiffness of the cracked lamina is known, the reduction of stiffness can be interpreted in terms of damage variables. Assuming damage in the form of a second order tensor with principal directions aligned with the c.s. of the cracked lamina, the degraded stiffness can be written as

$$Q_{ij} = \begin{bmatrix} Q_{11} & Q_{12} & 0 \\ Q_{12} & Q_{22} & 0 \\ 0 & 0 & Q_{66} \end{bmatrix} = \begin{bmatrix} (1-D_{11})Q_{11}^0 & (1-D_{12})Q_{12}^0 & 0 \\ (1-D_{12})Q_{12}^0 & (1-D_{22})Q_{22}^0 & 0 \\ 0 & 0 & (1-D_{66})Q_{66}^0 \end{bmatrix} \tag{18}$$

where Q_{ij}^0 are the coefficients of the intact lamina. In other words, the presence of the crack on the boundaries of the RVE (Figure 1) is homogenized. The damage variables can be calculated from the results of the analysis as

$$D_{ij} = 1 - Q_{ij}/Q_{ij}^0 \quad ; \quad i,j = 1,2,6 \tag{19}$$

Various hypothesis have been made in the literature about the relationship, or lack thereof, between the coefficients of the damage tensor. For example, [19,20] propose that the minor Poisson's ratio ν_{21} and the transverse modulus E_2 degrade at the same rate; in other words, that $D_{12} \approx D_{22}$.

Furthermore, [42], [43] propose that $D_{66} = 1 - (1-D_{11}^t)(1-D_{11}^c)(1-D_{22}^t)(1-D_{22}^c)$, where the superscripts t, c, indicate tension and compression. Since polymer matrix composites are relatively brittle in tension/compression along the longitudinal direction and in transverse compression, $D_{11}^t \approx D_{11}^c \approx D_{22}^2 \approx 0$, resulting in $D_{66} \approx D_{22}$. The present work allows us to asses these assumptions in the context of linear elastic behavior without the kinematic assumptions of other models in the literature.

Simultaneously with the laminate thermal analysis, the average thermal stress in the cracked lamina is obtained by averaging over the volume of the cracked lamina only, i.e.,

$$\overline{\sigma}_i^{(k)\ \text{thermal}} = \frac{\lambda}{t_k} \int_{V_k} \sigma_i dV \quad ; \quad \text{with } \epsilon_j = 0 \quad \forall j; \quad \Delta T = 1; \quad i = 1,2,6 \tag{20}$$

Once the averaged thermal stress in lamina (k) is known, the laminate coefficient of thermal expansion (CTE) of the craked lamina is calculated as

$$\alpha^{(k)} = \left(Q_{ij}^{(k)}\right)^{-1} \overline{\sigma}_j^{(k)\ \text{thermal}} \tag{21}$$

5 Implementation

Since periodic boundary conditions are not readily available in Abaqus, they were implemented in this work by developing a Python script for Abaqus/CAE 6.10-2. The script generates the RVE, meshes, then generates constrains in the faces that are periodic, and finally solves the model and stores the averaged stresses.

The script was validated against known solutions and experimental data. First, when no crack is present, the solution must coincide with Classical Lamination Theory (CLT). Since the strain and stresses in this case are piecewise constant throughout the body, no mesh refinement is necessary. Still, different meshes were used to verify that the solution does not change as a function of the number of nodes at the faces, i.e., the nodes that enforce both periodicity and the applied strain. With reference to Table 1, laminate #1 was used for this validation. The inplane degraded stiffness matrix predicted by CLT, in the laminate c.s., is defined as

$$Q_{ij}^{\mathrm{CLT}} = \frac{1}{t}\sum_{k=1}^{N} Q_{ij}^{(k)} t_k \quad ; \quad \text{with } i,j = 1,2,6 \tag{22}$$

where N is the number of laminas in the laminate and t, t_k, are the laminate and lamina thickness, respectively. For laminate #1 without any cracks (intact), (22) was calculated using [44]

$$Q_{ij,\text{ laminate c.s.}}^{\text{CLT, intact}} = \begin{bmatrix} 22108.664 & 9062.480 & 0 \\ 9062.480 & 26379.612 & 0 \\ 0 & 0 & 10993.620 \end{bmatrix} \tag{23}$$

The Q_{ij}^{CLT} matrix can be transformed to the c.s. of the cracked lamina by standard coordinate transformation [37, § 5.4.3], yielding

$$Q_{ij,\text{ lamina c.s.}}^{\text{CLT, intact}} = \begin{bmatrix} 27979.25 & 6057.74 & -90.29 \\ 6057.74 & 26518.51 & 2096.98 \\ -90.29 & 2096.98 & 7988.88 \end{bmatrix} \tag{24}$$

Therefore, the quality of the finite element simulation of intact laminate can be benchmarked by this result.

5.1 Intact RVE

The procedure followed to construct the model for the undamaged (intact) RVE is as follows:

1. Create the part: The python script generates an extruded square of dimensions $x = y = t_k$, $z = t$, The dimension in the x- and y-directions is chosen as the thickness of one lamina to have a good element's aspect ratio. Subsequently, the script creates a part embodying a 3D deformable body.

2. Define the material: An elastic material of type Engineering Constants is created and the properties from Table 2 are assigned to it.

3. Create the section: A homogenous solid section is created with the previous material.

4. Create the sets: In order to apply the boundary conditions a number of sets are defined, namely, the faces whose normal points either in x or y direction, positive or negative orientation, excluding the edges, and the edges between those faces. An algorithm was devised to search for these features using Python classes available in Abaqus/CAE.

5. Create the LSS: Planes are created to delimit the laminas. A datum plane is generated offsetting the xy-plane by the accumulated thickness. Immediately afterwards, the part is partitioned using those planes. The partition process creates a cell for each lamina in the laminate. A material orientation, relative to (k), is assigned to each cell. The section created in step 3, which is independent of the orientation, is then assigned to every cell.

6. Create the instance: A new instance is created in the root assembly and translated so the mid-plane is located at coordinate z=0.

7. Create the Step: The python script creates a new Static General step.

8. Define the Field Output Requests: The variables required for the analysis are requested from the solver: E (Strain), S (Stress), IVOL (Integration Volume), U (displacements).

9. Create a Reference Point: A reference point is created and a unit constant displacement is assigned to it. This point is necessary because the constraint equations in Abaqus relay on degrees of freedom. Since the periodic boundary conditions (equations (1)-(2)) contain a constant term that represents the applied strain, a degree of freedom is needed to apply such constrain throughout the simulation; this can only be achieved by using a Reference Point.

10. Create the Mesh: A C3D8 (8-node brick) or C3D20 (20-node brick) element for each layer is generated by the python script.

11. Restrain Rigid Body Motion: The node closer to the center of the RVE is fixed in x-, y-, and z-directions to prevent rigid body motion.

Once the RVE is constructed, the model is used as a template to generate each of the three cases, as follows:

1. The template model is copied to new models named *case-a*, *case-b*, *case-c*, and *case-d*.

2. Create Periodic Boundary Conditions for opposite faces. The procedure followed to pick the master and slave edges is as follows:

   (a) X axis: The face whose normal is in the direction of x positive is chosen as the master, while the face whose normal is in the negative direction is slave. The nodes in the slave face are searched to pair with the nodes in the master face. This is done by looping through the array of nodes in the master face and selecting the slave node with the minimum distance in the yz plane. Both faces, master and slave, must have the same number of nodes, which is not a problem for a parallelepiped RVE such as the one used in this study or when using a structured meshing algorithm. In the interaction module, a constraint equation, such as equations (1) or (2), is created for each direction (x, y and z). This equation relates the displacement of the master and the slave node with the displacement that results from the imposed strain field multiplied by unit displacement at the reference node.

   (b) Y axis: The same procedure used for the x axis is repeated for the y axis.

3. Create Periodic Boundary Conditions for edges. As explained before, the constraint equations at the edges are the combination of the equations at the intersecting faces. The procedure followed to pick the master and slave edges is as follows:

(a) In the xy plane (Figure 1) there are four edges and the equations have to relate two pairs: XmYm with XpYp and XmYp with XpYm. If we think of m as 0 and p as 1, then the pairs can be generated with a loop with i= 0,1 (the two pairs). The master is the loop index value i while the slave is the bitwise negation (word size is two bits).

(b) A truth table for this relation is shown in Table 3. This procedure automates the selection of pairs of edges in the python script.

(c) Once the master and slave edges have been defined, a pair algorithm is used to find the slave node for each master node. The algorithm looks for the pair with the minimum distance in the z direction.

(d) A constraint equation, such as equation (3) for XpYp-XmYm or (4) for XmYp-XpYm, is added to the model for each pair of master-slave nodes, relating the displacement in x-, and y-direction with the displacement that results from the imposed strain field.

4. Create job: A job is created and submitted. The number of physical processors is assigned to execute the job in parallel.

5. Get the Reduced Stiffness Matrix column: For each case, a, b, and c, in item 1, the field output corresponding to the stress in the c.s. of lamina (k), which is the global c.s. for the model, is looped over the integration points and an accumulation variable is incremented by the stress value times the integration volume. The same procedure is followed for the strain.

At the end of the loop, the total stresses and strains are divided by the total volume, yielding the average strains and stresses in the laminate. For each case, a, b, and c, the three components of stress yield the column 1, 2, and 3, of the degraded stiffness matrix of the laminate.

The degraded stiffness matrix for laminate #1, calculated using eight C3D8 elements and thirty-six nodes is obtained, in the c.s. of the cracked lamina, as

$$Q_{ij,\text{ lamina c.s.}}^{\text{CLT, intact}} = \begin{bmatrix} 27979.25 & 6057.74 & -90.29 \\ 6057.74 & 26518.51 & 2096.98 \\ -90.29 & 2096.98 & 7988.88 \end{bmatrix} \tag{25}$$

The accuracy of the FEA solution is measured by the number of significant digits to which the FEA result concides with the CLT result

$$\text{Significant}_{ij} = -\lg_{10} \frac{Q_{ij}^{\text{FEA}} - Q_{ij}^{\text{CLT}}}{Q_{ij}^{\text{CLT}}} \tag{26}$$

which, for laminate #1 yields

$$\text{Significant}_{ij} = \begin{bmatrix} 7 & 7 & 6 \\ 7 & 7 & 8 \\ 5 & 6 & 7 \end{bmatrix} \tag{27}$$

Equation (25) coincides with (24) up to single precision. Since Abaqus results are written in single precision, we conclude that no error is found between the Abaqus solution and the CLT solution. The homogenized (averaged) strains for each case are shown in Table 4. Note that all the zeros are zeros up to single precision accuracy and ones are ones up to single precision accuracy. The strain component 3 is not zero, thus confirming the plane stress state.

5.2 Cracked RVE

Once the procedure used to build the intact RVE has been validated, the damaged RVE was simulated. In this section, the differences with the intact template model are explained.

1. Create the Part: The RVE size in the y-direction is the inverse of the crack density because the cracks are assumed to be equally spaced along that direction by a distance $2l = 1/\lambda$. The RVE size in the x-direction is the minimum between the inverse of the crack density $(1/\lambda)$ and the lamina thickness (t_k), leading to elements with a good aspect ratio while minimizing the number of elements required for a good discretization.

2. Normalization: The lengths, elastic moduli, and coefficients of thermal expansion of the lamina are normalized by the maximum value of each type of data. This is done to minimize numerical errors. The scale factors are saved for subsequent use to denormalize the results.

3. Sub-laminate partition: Because the crack faces are normal to the y-axis, the periodicity in the faces normal to the y-axis is broken at the cracking laminas. Therefore, the part is divided in five cells so each cell can be treated separately:

   (a) Homogenized laminas below the (k) lamina (Lamina number 1 in Figure 2)

   (b) Cracked lamina (k) (Lamina number 2 in Figure 2)

   (c) Homogenized laminas between (k) and symmetric cracked lamina $(N + 1 - k)$, i.e., Laminas number 3 to 6 in Figure 2.

   (d) Cracked lamina $N + 1 - k$ (Lamina number 7 in Figure 2)

   (e) Homogenized laminas above the $N + 1 - k$ lamina (Lamina number 8 in Figure 2)

4. Create the sets:

   (a) In the homogenized cells (1, 3 and 5), constraints equations are set in pairs for the four faces whose normal is in the x- and y-directions, plus and minus orientation. This is done in the same fashion as in the intact case. The sets exclude the edges between the x- and y-faces. Those edges feature constraint equations that are the combination of the periodic boundary conditions for x- and y-faces (see (3)–(4)).

   (b) In the cracked lamina cells (2 and 4), constraint equations are set only for the faces whose normal is in x-direction, plus and minus direction. The sets exclude the edges between the x- and z-faces because these nodes were included in the homogenized cells sets. The cracks faces (normal in y-faces) are left unconstrained because they are stress free surfaces $(\sigma_2 = 0)$.

5. Create the LSS: Cells 1, 3, and 5 may contain several laminas, therefore these cells (or sub laminates) are partitioned further into laminas, and a similar procedure described for the intact case is followed for the assignment of the material orientation and section.

6. Create the mesh: The initial seed size is calculated based on the aspect ratio of the RVE, and then it is modified until the number of elements in the mesh is in the desired range that ensures accuracy and affordable computational time.

Similarly to the intact case, once the template model has been defined, each strain case is executed and the resultant homogenized stresses stored. The differences between the intact and cracked models are highlighted below.

1. Create Periodic Boundary Conditions in Homogenized Cells:

   (a) Face constraints: For each homogenized sub-laminate (1, 3, and 5) and for each normal axis (x and y) the nodes are paired following the procedure explained for the intact model. Afterwards, constrains equations in x, y, and z, are created between the nodes in the minus and plus orientation.

   (b) Vertical edge constraints: The same procedure to find the pair master-slave edges outlined in the intact model is followed for the x-y edges in the homogenized cells.

2. Create Periodic Boundary Conditions: in cracked (k) and ($N+1-k$) cells.

   (a) X Face constraints: For each cracking lamina (cells 2 and 4) the nodes in the faces whose normal is in the x-direction are paired following the procedure explained for the intact model. Afterwards, constrains equations in x, y, and z, are created between the nodes in the plus (p) or minus (m) orientations. The crack surfaces are left unconstrained.

6 Results

A mesh convergence study was performed for Laminate # 1 with crack density $\lambda = 1/t_k$. The percent error is calculated as

$$\%error = \frac{|Q_{11}(n) - Q_{11}(N)|}{Q_{11}(N)} \times 100 \tag{28}$$

where n, N, are the number of nodes of a given discretization and the maximum number of nodes, respectively. The % error is show in Figure 4. Computations were performed with $N = 3,390$ for C3D8 elements and $N = 1,000$ for C3D20 elements. As it can be seen in Figure 4, once a threshold number of elements is exceeded, the error decreases rapidly, converging to a negligible value. In this work, all the computations were performed, if at all possible in terms of displacements, which are more accurate than stresses in a displacement FEM formulation, and besides, they are stored as *double precision* in Abaqus.

A contour plot of normalized strain is shown in Figure 5, where the RVE is replicated eight times to aid the visualization. The strain field in the homogenized laminas matches the applied strain, while cracked laminas experience less deformation. In the proximity of the crack tip the strain increases up to 30% from the applied strain ($\epsilon_2 = 1.3$).

Calculated longitudinal laminate modulus vs. crack densities for laminates #1 and #6 are shown in Figures 6-7. Results for the remaining laminates listed in Table 1 are shown as additional material accompanying the online edition of this manuscript.

The asymptotic values of E_x for very low ($\lambda = 10^{-2}$) and very high ($\lambda = 10^3$) crack density coincide with the CLT solution obtained assuming that the cracked laminas are intact and fully damaged, respectively. In between those values, the FEA solution is the best solution available, in the sense that it is obtained with the minimum set of assumptions and simplifications. That is, a 3D elasticity problem of a periodically cracked media is discretized with a mesh that has been shown to yield negligible discretization error (Figure 4). The periodicity conditions are applied exactly as far as the discretization allows it. No other approximations are introduced. In this sense, the DDM solution is compared to the FEM solution, with the latter considered to be the benchmark solution. Note that DDM assumes linear distribution of intralaminar shear stress σ_4 and σ_5 in each lamina, while the FEM solution, with a large number of elements through the lamina thickness, does not impose any significant kinematic assumption.

Transverse laminate modulus E_y in laminate c.s. vs. crack density plots are shown in Figures 8-9. Again, the CLT solution validates the asymptotes and the FEM solution becomes the benchmark in between.

Note that, when compared to the intact value, the magnitude of degradation for Carbon/Epoxy (Figures 7 and 9) is very small. Such degradation would be very difficult to detect experimentally. Approximate models such as Abaqus and ANSYS progressive damage analysis (PDA) require modulus reduction data to adjust their phenomenological material parameters, i.e., the fracture energy [45]. Since modulus reduction is so difficult to detect experimentally, the identification of material parameters in approximated models such as those could be unreliable. An alternative is to generate modulus reduction data through simulation using the methodology proposed herein, namely (Figure 9), and use such simulation results to adjust the phenomenological parameters in the approximate model.

Apparent laminate coefficient of thermal expansion (CTE) in both x- and y-directions vs. crack density are shown in Figures 10-11 for laminates #1 and #6, respectively. Unlike the laminate CTE shown in Figures 10-11, the cracked lamina CTE remains constant for the six laminates analyzed, i.e., $\alpha^{(k)} = constant$.

Experimental results are compared to the FEA solution in Figures 12-13 for laminate #2, displaying good agreement.

All the comparisons, including those reported in the online edition, are good. The comparison experimental data to FEM is good. The comparison of DDM to FEM is good. The most notable difference occurs in the Poisson's ratio versus crack density shown in Figure 14 for laminate #3 when the crack spacing is about seven lamina thickness, but even then, the difference is small.

The damage variables calculated with (19) for laminate #1 and #6 are shown in Figures 15-16. Again, the DDM solution is close to the FEM benchmark. Note in Figures 17-18 that $D_{12} = D_{22}$ for all values of crack densities. Therefore

$$\frac{Q_{12}}{Q_{22}} = \nu_{12} = constant \tag{29}$$

Since $E_1 \approx$ constant, then $\nu_{21}/E_2 =$ constant, which agrees with the hypothesis in [19, 20] that is also used in several damage models such as [46–48]. While the major Poisson's ratio of the lamina ν_{12} remains constant, the Poisson's ratio of the laminate ν_{xy} does degrade as shown in Figures 13–14.

Also, it can be observed in Figures 19-20 that although D_{66} is not exactly equal to D_{22}, it is not far from it either, thus supporting the assumption indirectly made in [42, 43], i.e., that $D_{66} = D_{22}$.

7 Conclusions

The proposed benchmark solution is validated by the CLT solution for asymptotic values of crack density. Also, experimental data compares well with the FEM solution. Confirmation is provided for the hypothesis that $D_{12} = D_{22}$, for all of the six laminates reported, which include both Glass/Epoxy and Carbon/Epoxy laminates. A novel finding is provided showing that $D_{66}/D_{22} \approx 1$ for all of the six laminates reported. Also, the cracking lamina CTE was found to be remain constant, i.e., unaffected by crack density. The comparison between the approximate DDM solution and FEM solution reveals that the shortcomings introduced by the approximations in DDM are not severe. The results provided can be used to benchmark the accuracy of approximate solutions. The procedure can be applied to generate additional results for other laminates. Since modulus reduction of Carbon/Epoxy is difficult to detect experimentally, the identification of material parameters in approximated models such as PDA could be based on modulus reduction results generated through simulation using the methodology proposed herein.

Future work may implement a global-local strategy where the proposed methodology provides the local solution. However, this would require additional effort, as explained in [49]. The model presented herein only provides the degraded stiffness of any lamina for a given crack density in that lamina. Calculating the crack density as a function of the applied loads (stress, strain, or temperature), requires additional considerations (see for example [50]). The degraded stiffness calculated at the local level by the model presented herein can then be used as homogenized properties in any type of laminated element, such as laminated shell or solid elements, at the global level. Additional work would be required to account for localization at the global level. Finally, the tangent stiffness could be calculated by numerical differentiation, based on the secant stiffness provided by the current model.

Acknowledgments

The authors wish to thank Rene Sprunger from 3DS for facilitating a teaching grant for Abaqus that allowed the first author to teach Abaqus and the other authors to learn it.

Figures

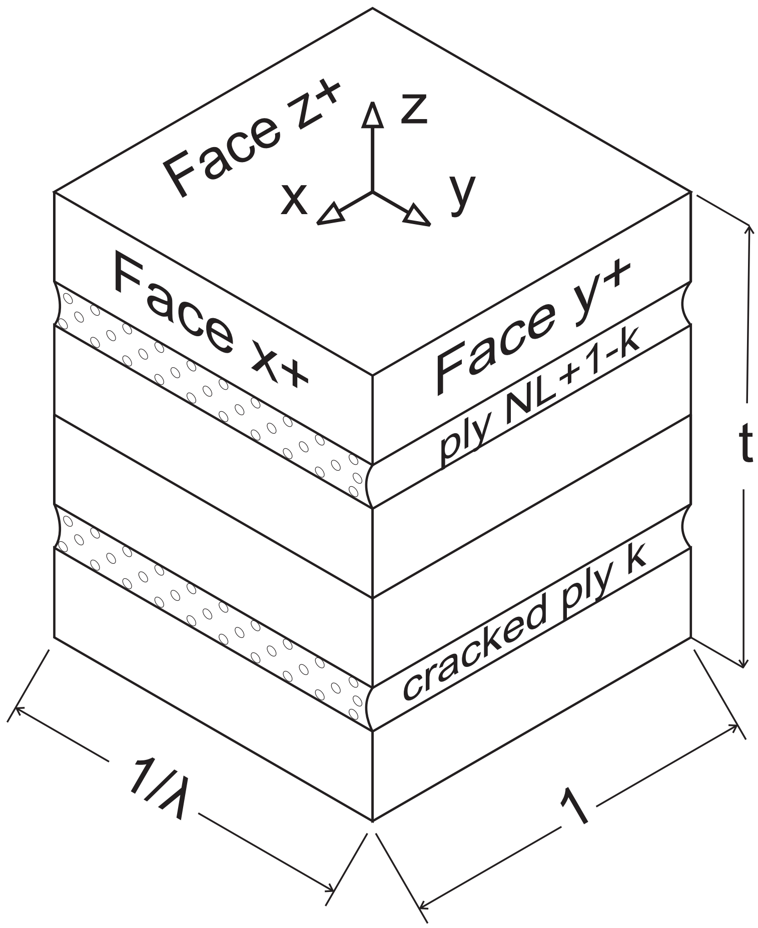

Figure 1: Representative volume element (RVE).

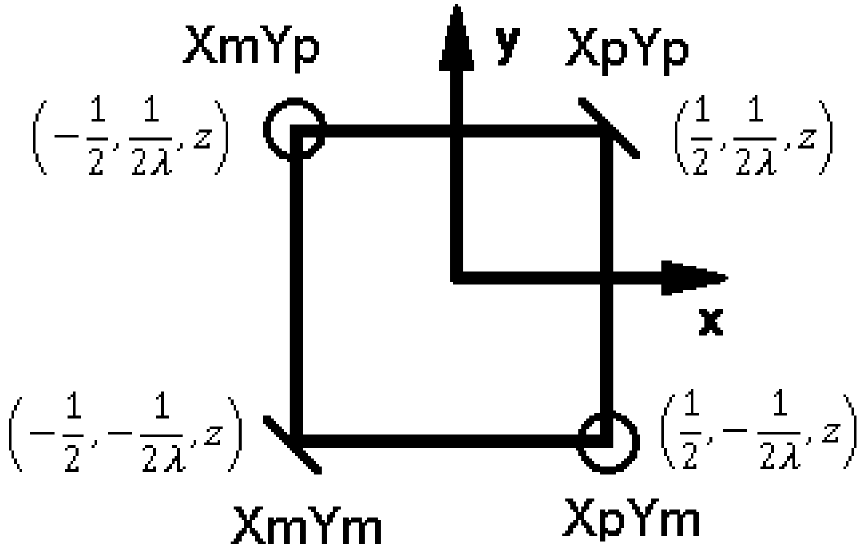

Figure 2: Labeling the edges.

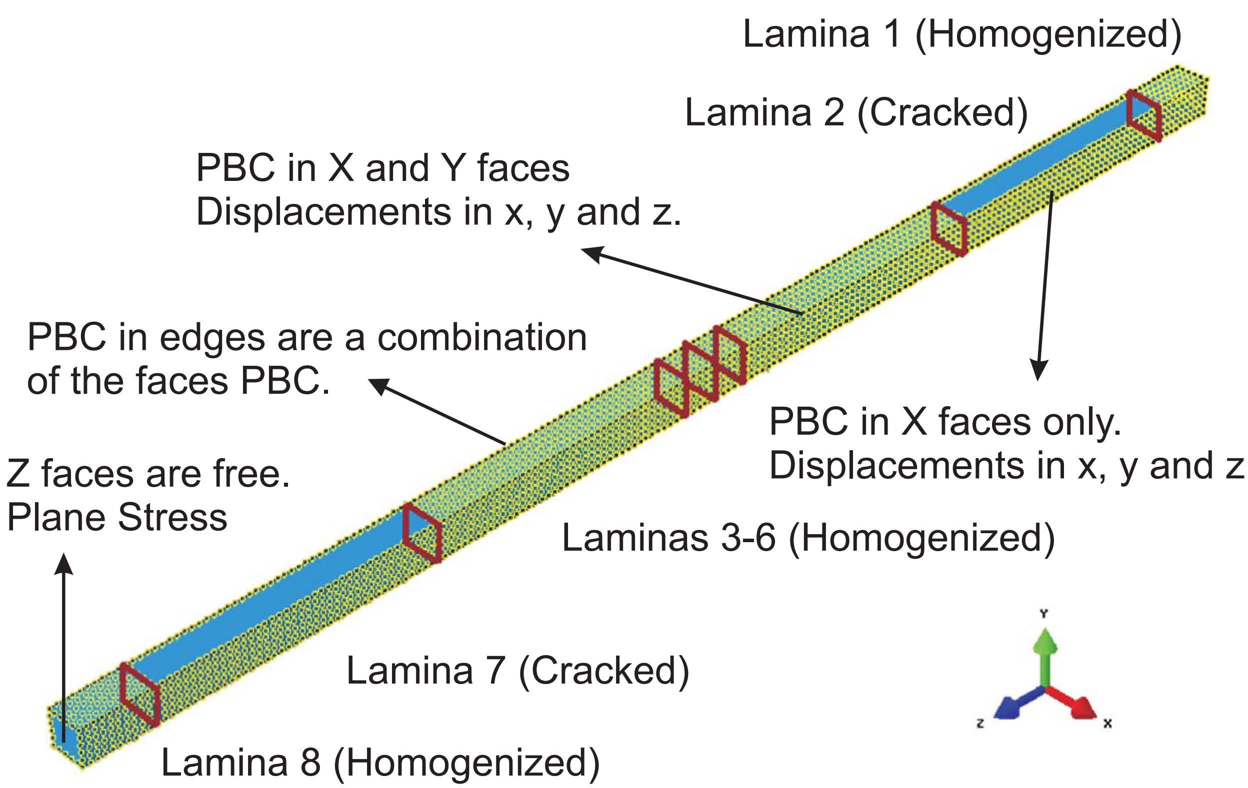

Figure 3: Solid model showing the boundary conditions.

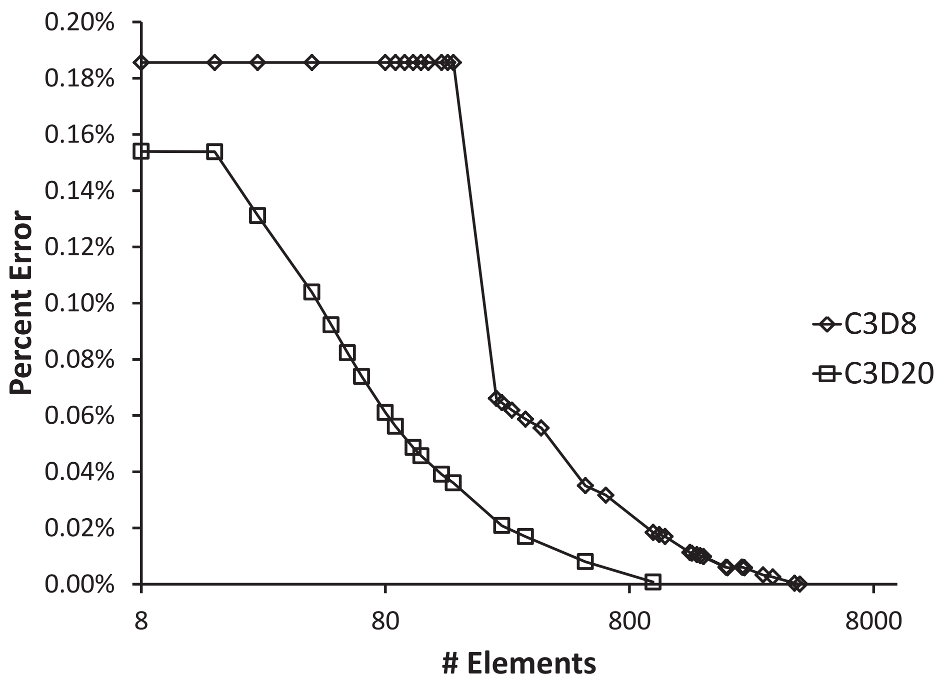

Figure 4: Convergence study. Percentage error vs. log number of elements.

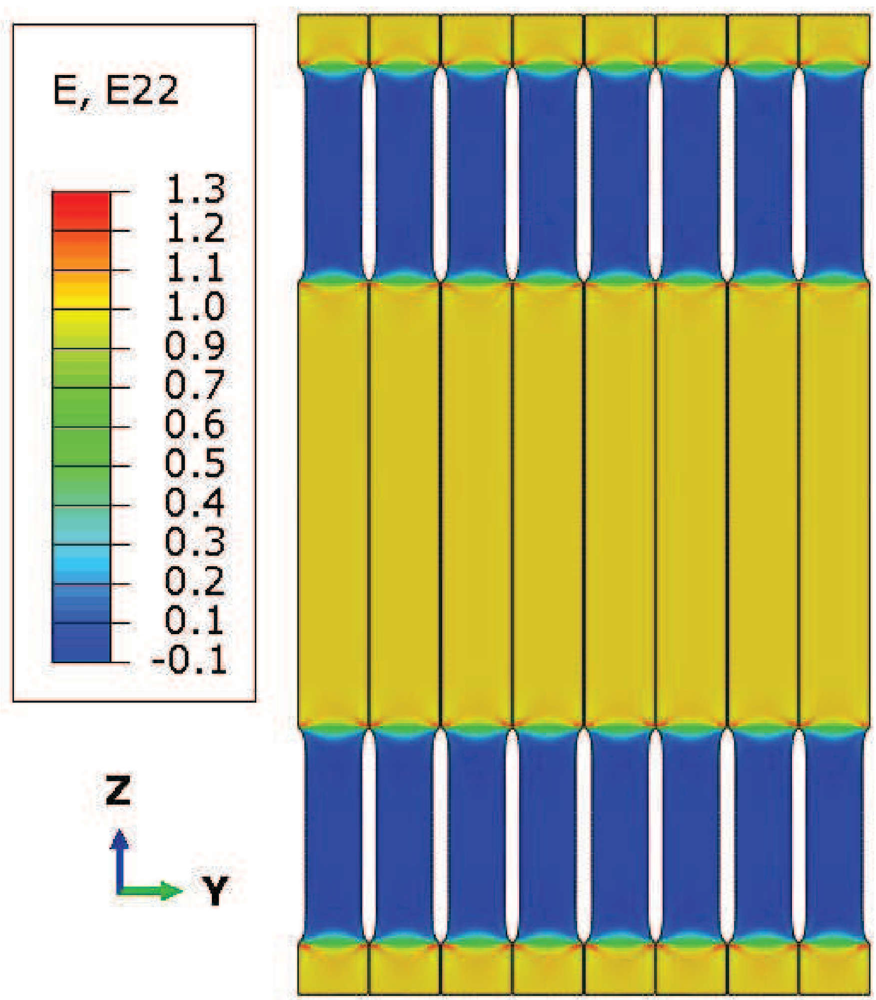

Figure 5: Strain field in eight consecutive RVEs for $\epsilon_2^0 = 1$.

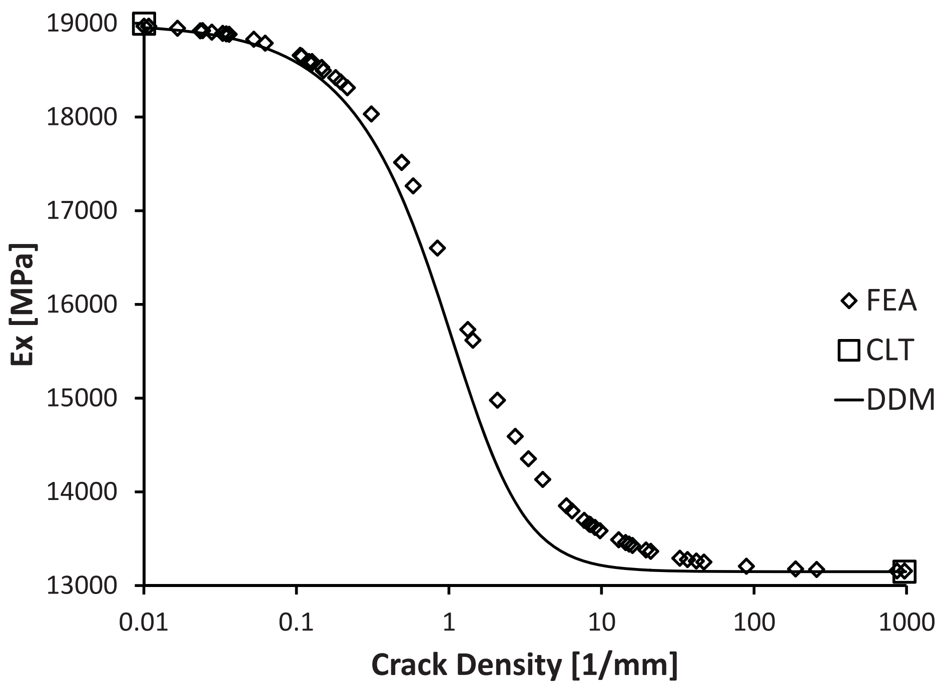

Figure 6: E_x vs. crack density for laminate #1.

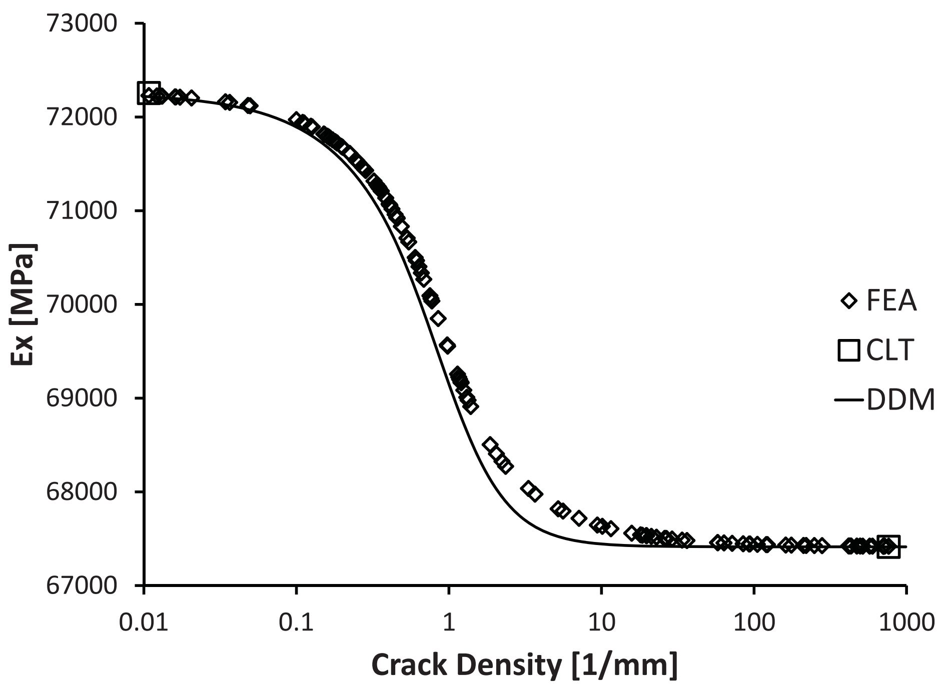

Figure 7: E_x vs. crack density for laminate #6.

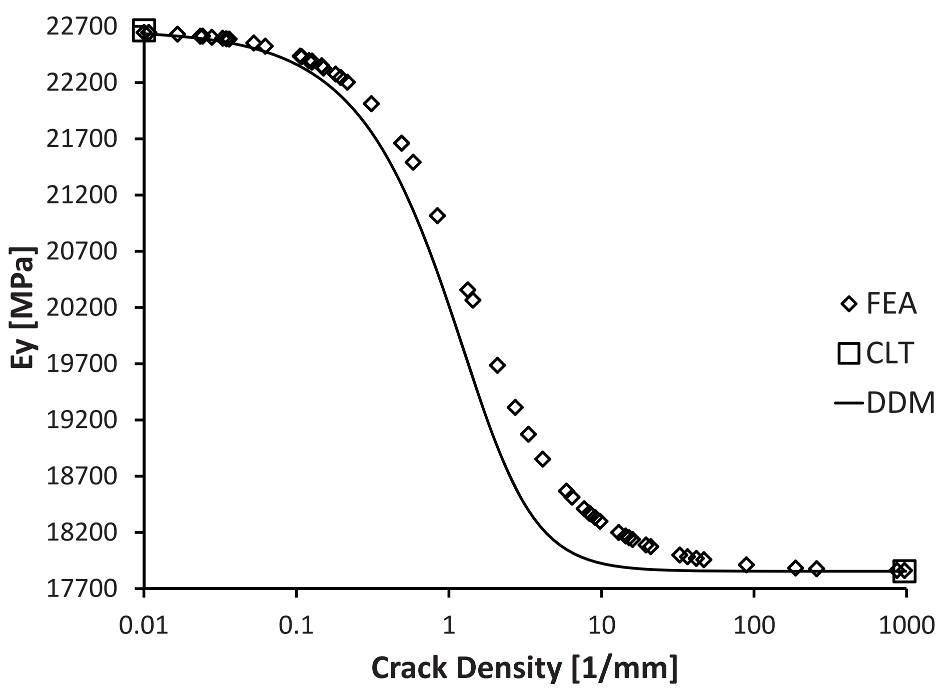

Figure 8: E_y vs. crack density for laminate #1.

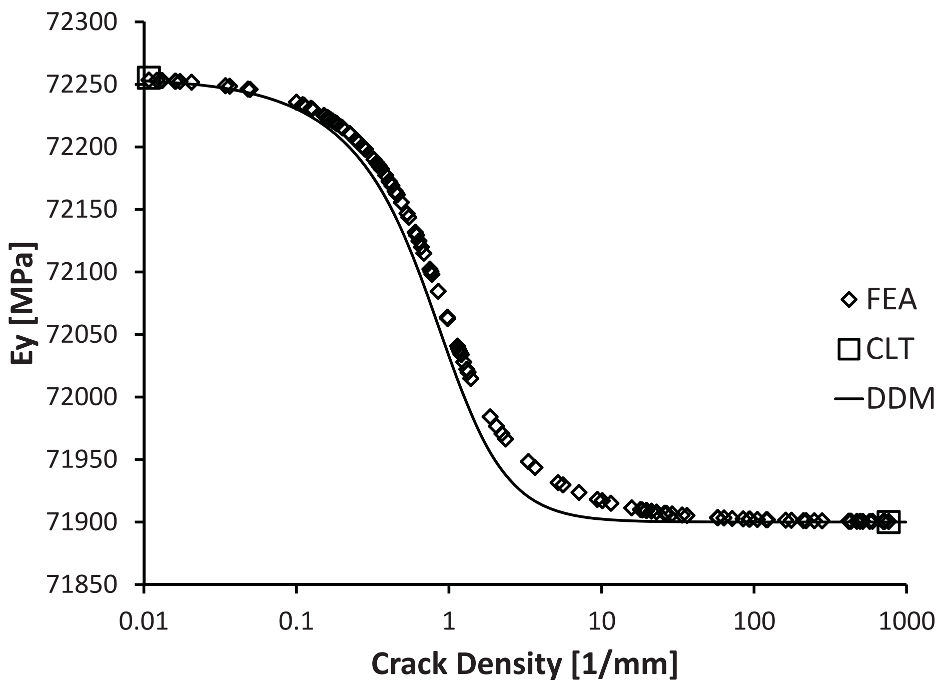

Figure 9: E_y vs. crack density for laminate #6.

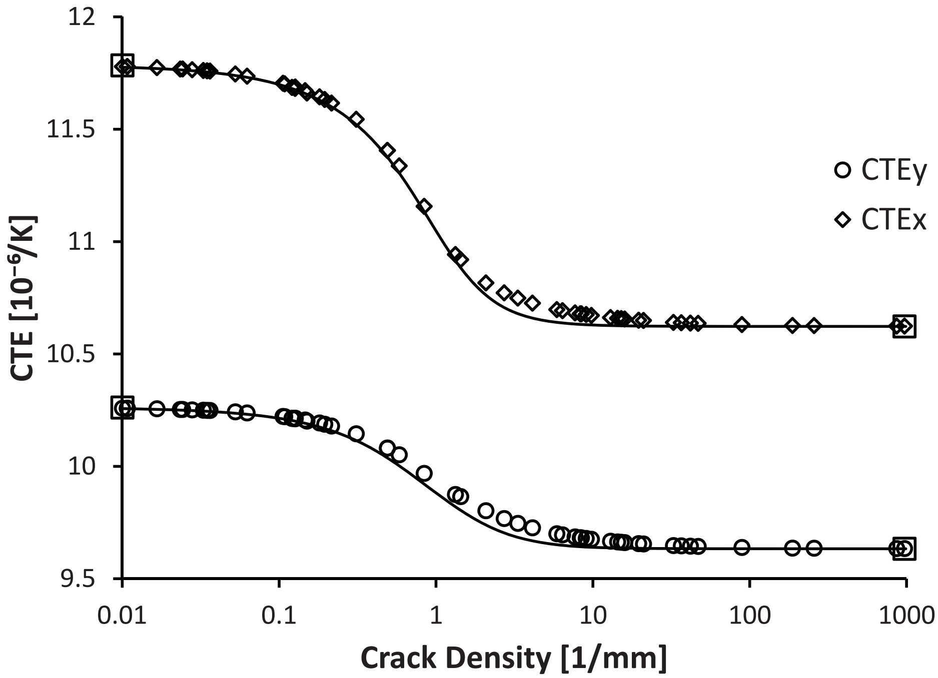

Figure 10: CTE α_x and α_y vs. crack density for laminate #1.

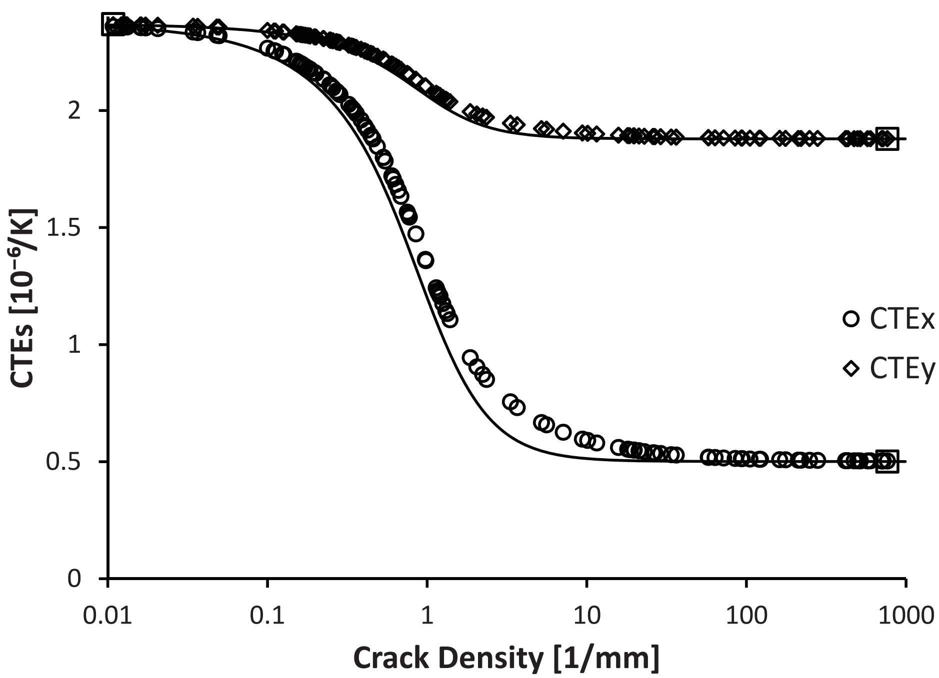

Figure 11: CTE α_x and α_y vs. crack density for laminate #6.

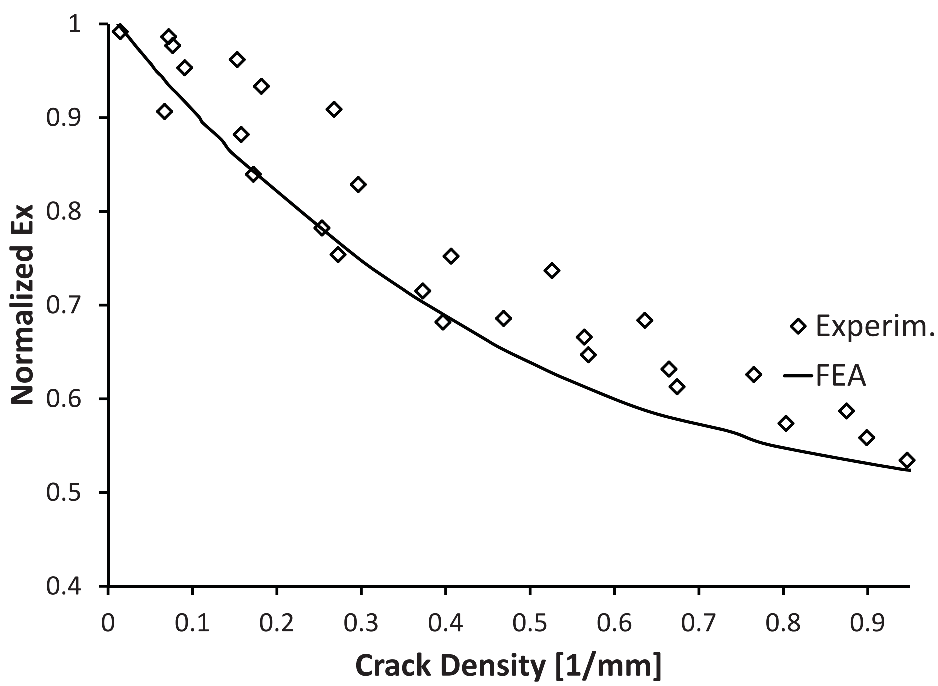

Figure 12: Laminate modulus E_x (normalized by the intact value) vs. crack density for laminate #2.

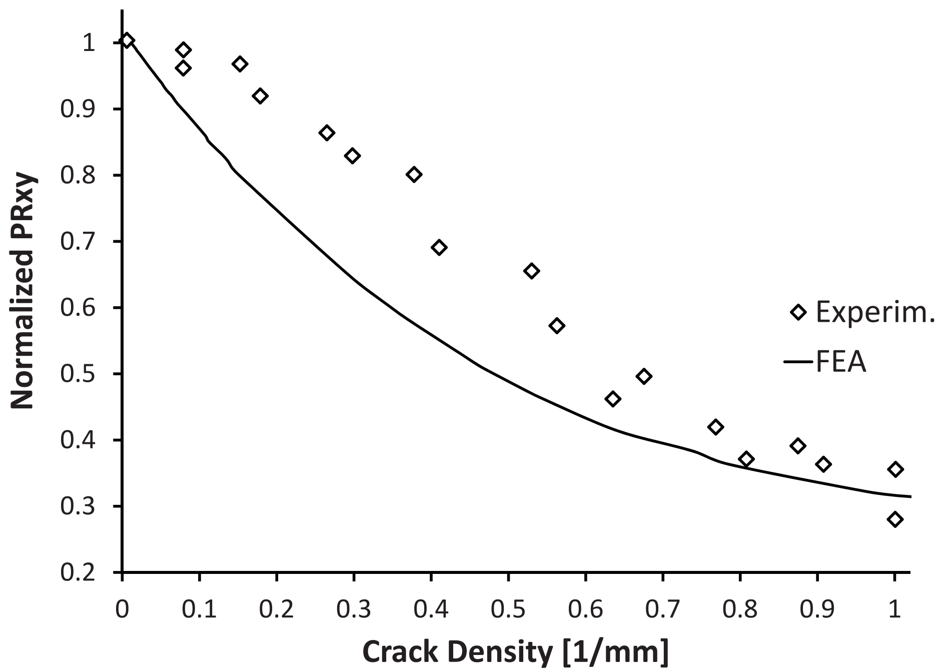

Figure 13: Laminate Inplane Poisson's ratio ν_{xy} (normalized by the intact value) vs. crack density for laminate #2.

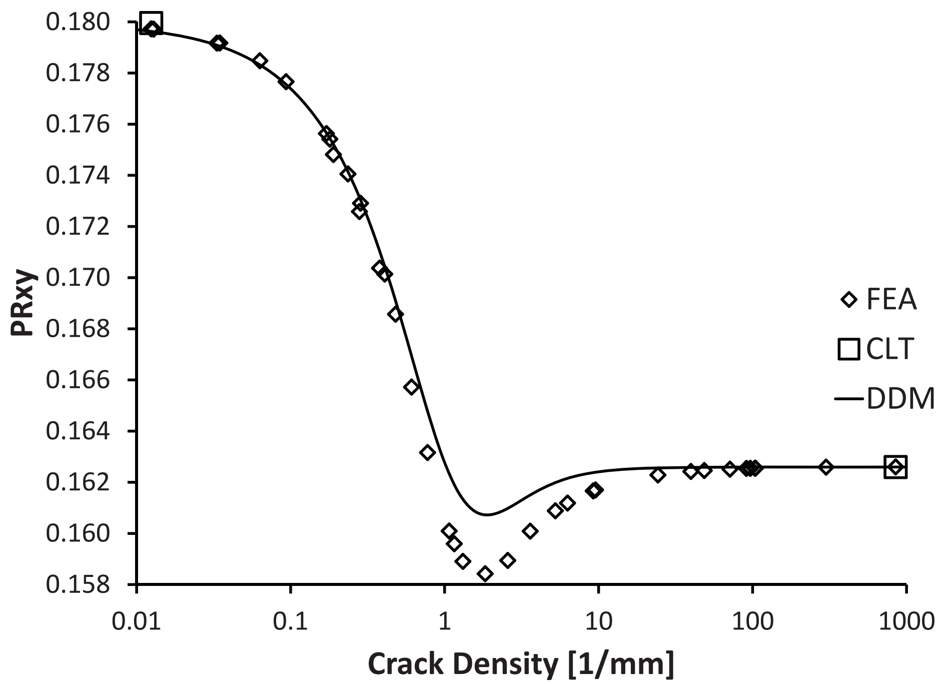

Figure 14: Inplane Poisson's ratio ν_{xy} vs. crack density for laminate 3.

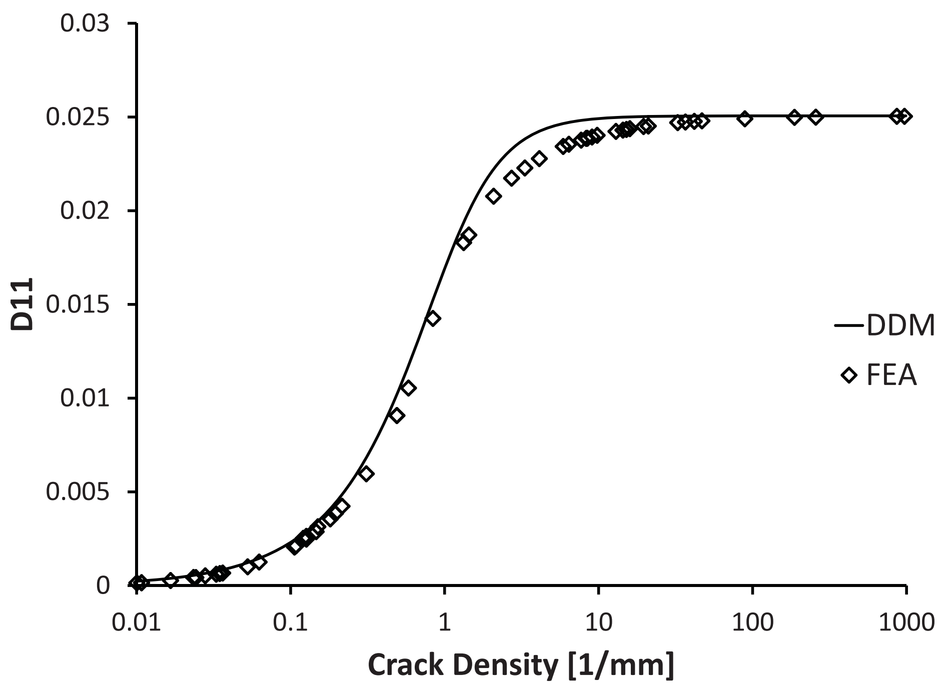

Figure 15: Damage D_{11} vs. crack density for Laminate #1.

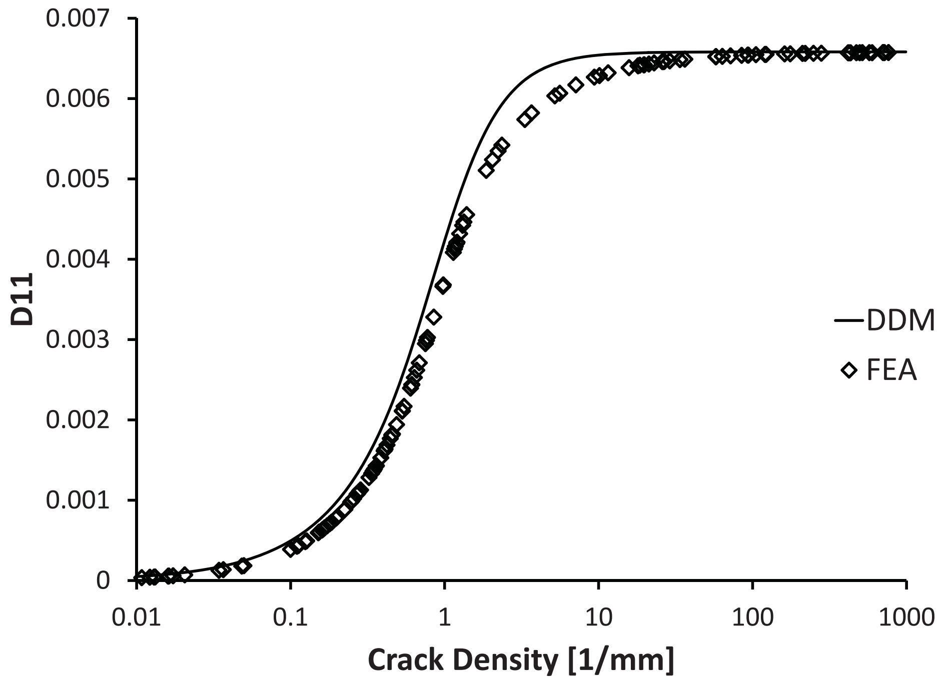

Figure 16: Damage D_{11} vs. crack density for Laminate #6.

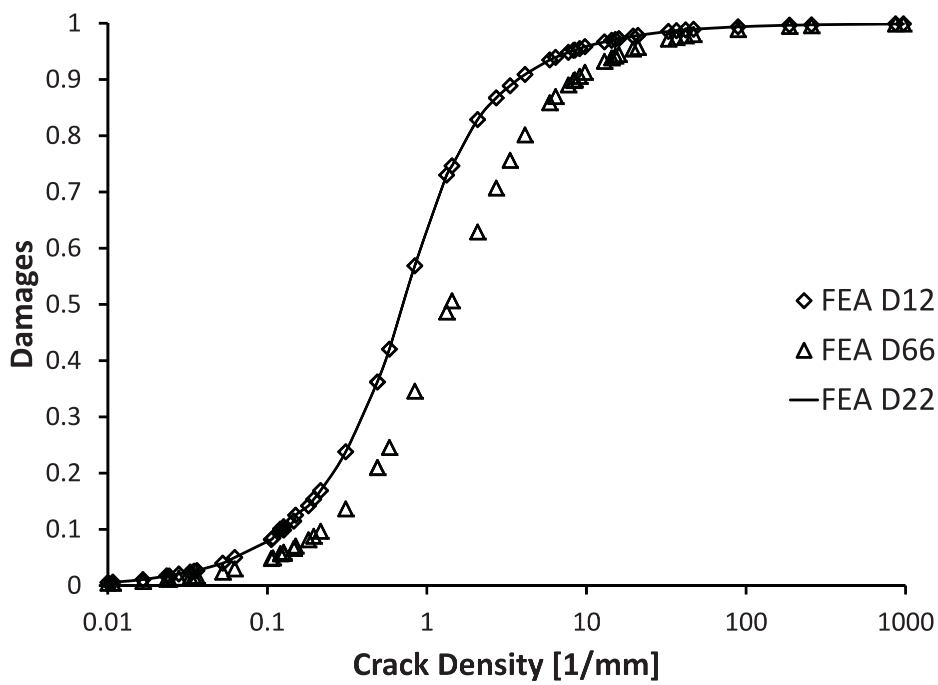

Figure 17: Damage D_{22}, D_{12}, and D_{66} vs. crack density for Laminate #1.

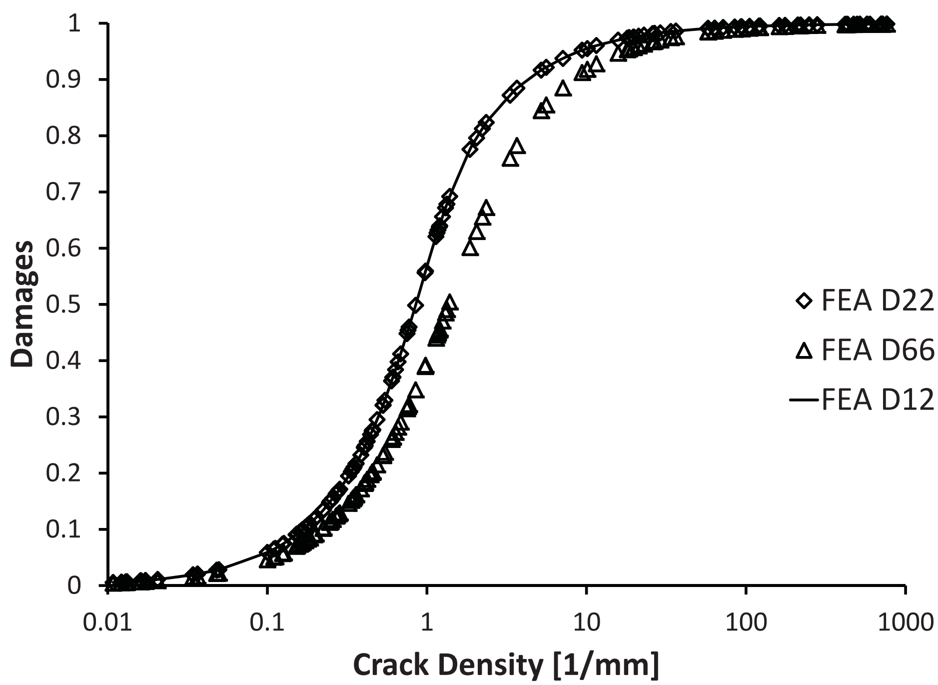

Figure 18: Damage D_{22}, D_{12}, and D_{66} vs. crack density for Laminate #6.

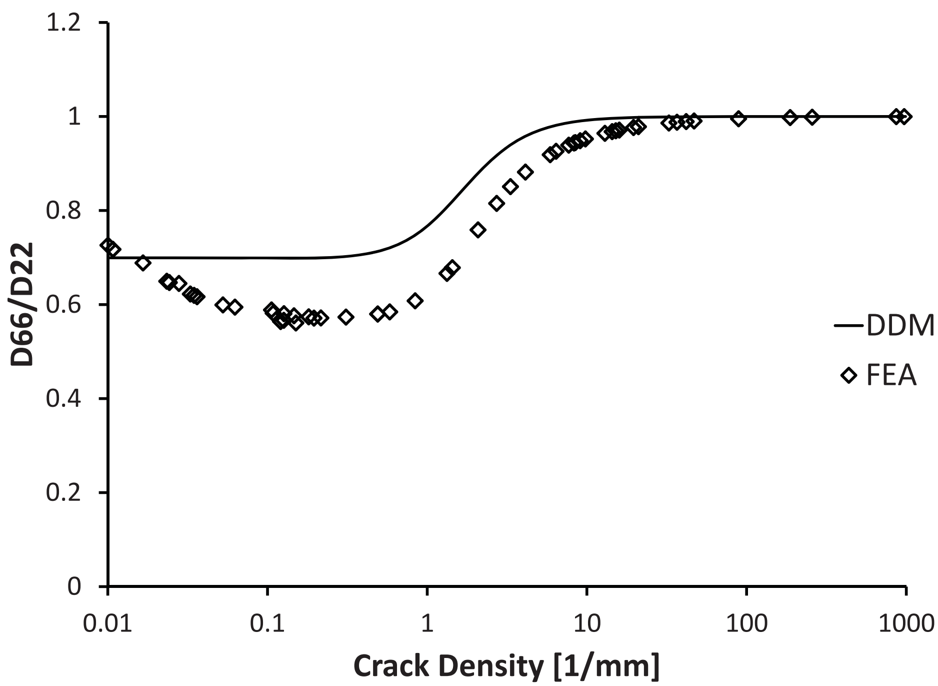

Figure 19: D_{66}/D_{22} for laminate #1.

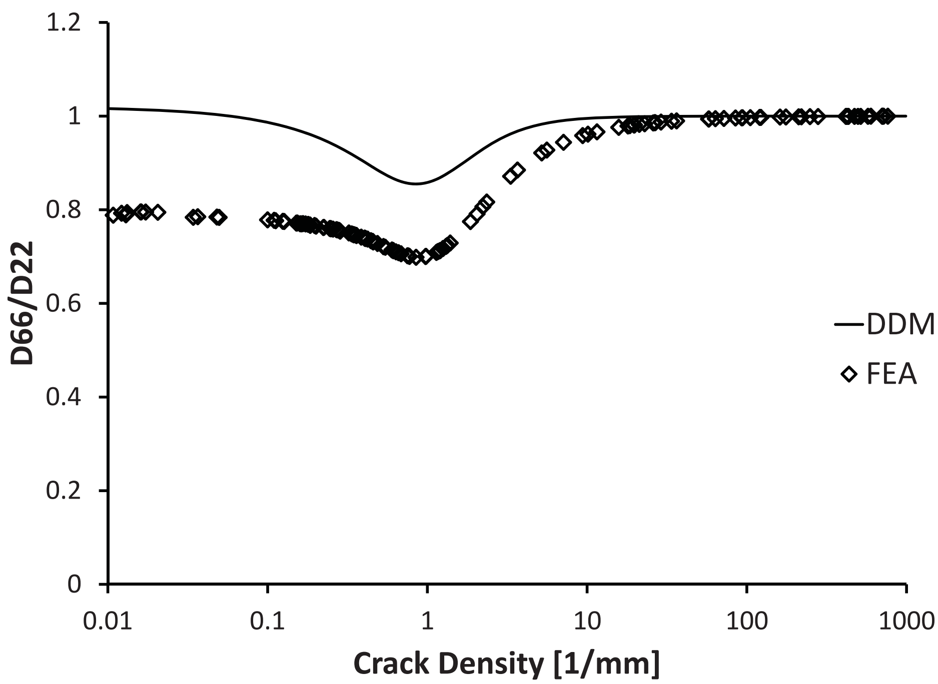

Figure 20: D_{66}/D_{22} for laminate #6.

Tables

Table 1: Laminates and materials.

Laminate	Stacking Sequence	Material	Reference
1	$[0/55_4/-55_4/0_{1/2}]_S$	Fiberite/HyE 9082Af	[51]
2	$[0/90_8/0_{1/2}]_S$		
3	$[0/70_4/-70_4/0_{1/2}]_S$		
4	$[0/90_2]_S$	Avimid K Polymer/IM6	[2]
5	$[0/90_3]_S$		
6	$[0_2/90_2]_S$		

Table 2: Material properties.

Property	Fiberite/HyE 9082Af [51]	Avimid K Polymer/IM6 [2]
E_1 [GPa]	44.7	134
E_2 [GPa]	12.7	9.8
G_{12} [GPa]	5.8	5.5
ν_{12}	0.297	0.3
G_{23} [GPa]	4.5	3.6
α_1 [10-6/K]	8.42	-0.09
α_2 [10-6/K]	18.4	28.8
t_k [mm]	0.144	0.144

Table 3: Truth table used to find the slave edges corresponding to chosen master edges.

i	Binary	Negated Binary	Master	Slave
0	00 or mm	11 or pp	XmYm	XpYp
1	01 or mp	10 or pm	XmYp	XpYm

Table 4: Averaged strains for the three cases. Intact laminate #1.

	Case (a)	Case (b)	Case (c)
ϵ_1	1+4E-08	-8E-09	-1E-08
ϵ_2	-8E-09	1+4E-08	1E-08
ϵ_3	-0.43	-0.43	0.00058
ϵ_6	4E-08	-6E-09	1+4E-08
ϵ_5	-2E-16	-8E-16	7E-16
ϵ_4	-9E-15	-1E-14	6E-15

References

[1] J. A. Nairn and S. Hu. *Damage Mechanics of Composite Materials*, volume 9 of *Composite Materials Series*, chapter Matrix Microcracking, pages 187–244. Elsevier, 1994.

[2] S. Liu and J. A. Nairn. The formation and propagation of matrix microcracks in cross-ply laminates during static loading. *Journal of Reinforced Plastics and Composites*, 11(2):158–78, 02 1992.

[3] J. A. Nairn. *Polymer Matrix Composites*, volume 2 of *Comprehensive Composite Materials*, chapter Matrix Microcracking in Composites, pages 403–432. Elsevier Science, 2000.

[4] J. A. Nairn. The strain energy release rate of composite microcracking: a variational approach. *Journal of Composite Materials*, 23(11):1106–29, 11 1989.

[5] J. A. Nairn, S. Hu, S. Liu, and J. S. Bark. The initiation, propagation, and effect of matrix microcracks in cross-ply and related laminates. In *Proc. of the 1st NASA Advanced Comp. Tech. Conf.*, pages 497–512, Oct. 29 - Nov. 1, 1990 1990.

[6] J. A. Nairn. Microcracking, microcrack-induced delamination, and longitudinal splitting of advanced composite structures. Technical Report NASA Contractor Report 4472, 1992.

[7] J. A. Nairn. Applications of finite fracture mechanics for predicting fracture events in composites. In *5th Int'l Conf. on Deform. and Fract. of Comp.*, 18-19 March 1999.

[8] J. A. Nairn. Fracture mechanics of composites with residual stresses, imperfect interfaces, and traction-loaded cracks. In *Workshop 'Recent Advances in Continuum Damage Mechanics for Composites'*, volume 61, pages 2159–67, UK, 20-22 Sept. 2000. Elsevier.

[9] J. A. Nairn and D. A. Mendels. On the use of planar shear-lag methods for stress-transfer analysis of multilayered composites. *Mechanics of Materials*, 33(6):335–362, 2001.

[10] J. A. Nairn. *Finite Fracture Mechanics of Matrix Microcracking in Composites*, pages 207–212. Application of Fracture Mechanics to Polymers, Adhesives and Composites. Elsevier, 2004.

[11] Y. M. Han, H. T. Hahn, and R. B. Croman. A simplified analysis of transverse ply cracking in cross-ply laminates. *Composites Science and Technology*, 31(3):165–177, 1988.

[12] C. T. Herakovich, J. Aboudi, S. W. Lee, and E. A. Strauss. Damage in composite laminates: Effects of transverse cracks. *Mechanics of Materials*, 7(2):91–107, 11 1988.

[13] J. Aboudi, S. W. Lee, and C. T. Herakovich. Three-dimensional analysis of laminates with cross cracks. *Journal of Applied Mechanics, Transactions ASME*, 55(2):389–397, 1988.

[14] F. W. Crossman, W. J. Warren, A. S. D. Wang, and G. E. Law. Initiation and growth of transverse cracks and edge delamination in composite laminates. ii - experimental correlation. *Journal of Composite Materials Suplement*, 14(1):88–108, 1980.

[15] D. L. Flaggs and M. H. Kural. Experimental determination of the in situ transverse lamina strength in graphite/epoxy laminates. *Journal of Composite Materials*, 16:103–16, 03 1982.

[16] S. H. Lim and S. Li. Energy release rates for transverse cracking and delaminations induced by transverse cracks in laminated composites. *Composites Part A*, 36(11):1467–1476, 2005.

[17] S. Li and F. Hafeez. Variation-based cracked laminate analysis revisited and fundamentally extended. *International Journal of Solids and Structures*, 46(20):3505–3515, 2009.

[18] J. L Rebiere and D. Gamby. A decomposition of the strain energy release rate associated with the initiation of transverse cracking, longitudinal cracking and delamination in cross-ply laminates. *Composite Structures*, 84(2):186–197, 2008.

[19] S. C. Tan and R. J. Nuismer. A theory for progressive matrix cracking in composite laminates. *Journal of Composite Materials*, 23:1029–1047, 1989.

[20] R. J. Nuismer and S. C. Tan. Constitutive relations of a cracked composite lamina. *Journal of Composite Materials*, 22:306–321, 1988.

[21] T. Yokozeki and T. Aoki. Stress analysis of symmetric laminates with obliquely-crossed matrix cracks. *Advanced Composite Materials*, 13(2):121–40, 2004.

[22] T. Yokozeki and T. Aoki. Overall thermoelastic properties of symmetric laminates containing obliquely crossed matrix cracks. *Composites Science and Technology*, 65(11-12):1647–54, 2005.

[23] P. Gudmundson and S. Ostlund. First order analysis of stiffness reduction due to matrix cracking. *Journal of Composite Materials*, 26(7):1009–30, 1992.

[24] P. Gudmundson and S. Ostlund. Prediction of thermoelastic properties of composite laminates with matrix cracks. *Composites Science and Technology*, 44(2):95–105, 1992.

[25] P. Gudmundson and W. Zang. An analytic model for thermoelastic properties of composite laminates containing transverse matrix cracks. *International Journal of Solids and Structures*, 30(23):3211–31, 1993.

[26] E. Adolfsson and P. Gudmundson. Thermoelastic properties in combined bending and extension of thin composite laminates with transverse matrix cracks. *International Journal of Solids and Structures*, 34(16):2035–60, 06 1997.

[27] E. Adolfsson and P. Gudmundson. Matrix crack initiation and progression in composite laminates subjected to bending and extension. *International Journal of Solids and Structures*, 36(21):3131–3169, 1999.

[28] W. Zang and P. Gudmundson. Damage evolution and thermoelastic properties of composite laminates. *International Journal of Damage Mechanics*, 2(3):290–308, 07 1993.

[29] E. Adolfsson and P. Gudmundson. Matrix crack induced stiffness reductions in [(0m/90n/+p/-q)s]m composite laminates. *Composites Engineering*, 5(1):107–23, 1995.

[30] P. Lundmark and J. Varna. Modeling thermo-mechanical properties of damaged laminates. In *3rd International Conference on Fracture and Damage Mechanics, FDM 2003*, volume 251-252 of *Advances in Fracture and Damage Mechanics*, pages 381–7, Switzerland, 2-4 Sept. 2003. Trans Tech Publications.

[31] M. Kachanov. volume 30 of *Advances in Applied Mechanics*, chapter Elastic solids with many cracks and related problems, pages 260–445. Academic Press, Inc., 1993.

[32] Z. Hashin. Analysis of cracked laminates: a variational approach. *Mechanics of Materials*, 4:121:136, 1985.

[33] J. Zhang, J. Fan, and C. Soutis. Analysis of multiple matrix cracking in $[\pm\theta/90_n]_s$ composite laminates, part I, inplane stiffness properties. *Composites*, 23(5):291–304, 1992.

[34] T. Yokozeki, T. Aoki, and T. Ishikawa. Transverse crack propagation in the specimen width direction of cfrp laminates under static tensile loadings. *Journal of Composite Materials*, 36(17):2085–99, 2002.

[35] T. Yokozeki, T. Aoki, and T. Ishikawa. Consecutive matrix cracking in contiguous plies of composite laminates. *International Journal of Solids and Structures*, 42(9-10):2785–802, 05 2005.

[36] T. Yokozeki, T. Aoki, T. Ogasawara, and T. Ishikawa. Effects of layup angle and ply thickness on matrix crack interaction in contiguous plies of composite laminates. *Composites Part A (Applied Science and Manufacturing)*, 36(9):1229–35, 2005.

[37] E. J. Barbero. *Introduction to Composite Materials Design–Second Edition.* CRC Press, Philadelphia, PA, 1st edition, 2010.

[38] E. J. Barbero. *Finite Element Analysis of Composite Materials.* Taylor & Francis, 2007.

[39] Fabrizio Greco. Homogenized mechanical behavior of composite micro-structures including micro-cracking and contact evolution. *Engineering Fracture Mechanics*, 76(2):182 – 208, 2009.

[40] Fabrizio Greco, Lorenzo Leonetti, and Paolo Nevone Blasi. Non-linear macroscopic response of fiber-reinforced composite materials due to initiation and propagation of interface cracks. *Engineering Fracture Mechanics*, 80(0):92 – 113, 2012. Special Issue on Fracture and Contact Mechanics for Interface Problems.

[41] S. Nemat-Nasser and M. Hori. *Micromechanics: overall properties of heterogeneous materials.* North Holland, 1993.

[42] AbaqusV6.1, Analysis User's Manual, Providence, RI, USA: Abaqus Inc, 2010.

[43] A. Matzenmiller, J. Lubliner, and R. Taylor. A constitutive model for anisotropic damage in fiber-composites. *Mechanics of Materials*, 20:125–152, 1995.

[44] E. J. Barbero. Computer aided design environment for composites. http:/www.cadec-online.com, 2011.

[45] E. J. Barbero, F. A. Cosso, R. Roman, and T. L. Weadon. Determination of material parameters for Abaqus progressive damage analysis of E-Glass Epoxy laminates. *Composites Part B:Engineering*, 2012.

[46] George J. Dvorak, Norman Laws, and Mehdi Hejazi. Analysis of progressive matrix cracking in composite laminates - i. thermoelastic properties of a play with cracks. *Journal of Composite Materials*, 19(3):216–234, 1985. cited By (since 1996) 44.

[47] B.N. Nguyen. Three-dimensional modeling of transverse matrix cracking in laminated composites. *Key Engineering Materials*, 127-131(Pt 2):1117–1126, 1997. cited By (since 1996) 2.

[48] N. Laws, G.J. Dvorak, and M. Hejazi. Stiffness changes in unidirectional composites caused by crack systems. *Mechanics of Materials*, 2(2):123–137, 1983. cited By (since 1996) 85.

[49] Fabrizio Greco, Lorenzo Leonetti, and Paolo Lonetti. A two-scale failure analysis of composite materials in presence of fiber/matrix crack initiation and propagation. *Composite Structures*, 95(0):582–597, 2013.

[50] E. Barbero and D. Cortes. A mechanistic model for transverse damage initiation, evolution, and stiffness reduction in laminated composites. *Composites Part B*, 41:124–132, 2010.

[51] J. Varna, R. Joffe, N. Akshantala, and R. Talreja. Damage in composite laminates with off-axis plies. *Composites Science and Technology*, 59:2139–2147, 1999.